# Investigation of the Electrocatalytic Reduction of Peroxydisulfate Using Scanning Electrochemical Microscopy

Seyyedamirhossein Hosseini<sup>1</sup>, Gergely T. Solymosi<sup>2,1</sup>, Henry S. White<sup>1\*</sup>

#### **Affiliations:**

<sup>1</sup> Department of Chemistry, University of Utah, 315 South 1400 East, Salt Lake City, Utah 84112, United States

<sup>2</sup> Department of Inorganic and Analytical Chemistry, Faculty of Chemical Technology and Biotechnology, Budapest University of Technology and Economics, Műegyetem rkp. 3, H-1111 Budapest, Hungary

\*Corresponding authors: white@chemistry.utah.edu

**Abstract**: The elementary steps of the electrocatalytic reduction of  $S_2O_8^{2-}$  using the Ru(NH<sub>3</sub>) $_6^{3+/2+}$ redox couple were investigated using scanning electrochemical microscopy (SECM) and steadystate voltammetry (SSV). SECM investigations were carried out in a 0.1 M KCl solution using a 3.5-µm radius carbon ultramicroelectrode (UME) as the SECM tip and a 25-µm radius platinum UME as the substrate electrode. Approach curves were recorded in the positive feedback mode of SECM by reducing Ru(NH<sub>3</sub>)<sub>6</sub><sup>3+</sup> at the tip electrode and oxidizing Ru(NH<sub>3</sub>)<sub>6</sub><sup>2+</sup> at the substrate electrode, as a function of the tip-substrate separation and S<sub>2</sub>O<sub>8</sub><sup>2-</sup> concentration. The one-electron reaction between electrogenerated  $Ru(NH_3)_6^{2+}$  and  $S_2O_8^{2-}$  yields the unstable  $S_2O_8^{3-}$ , which rapidly dissociates to produce highly oxidizing SO<sub>4</sub>. Because SO<sub>4</sub> is such a strongly oxidizing species, it can be further reduced at both the tip or the substrate, or it can react with  $Ru(NH_3)_6^{2+}$  to regenerate Ru(NH<sub>3</sub>)<sub>6</sub><sup>3+</sup>. SECM approach curves display a complex dependence on the tip-substrate distance, d, due to redox mediation reactions at both the tip and the substrate. Finite element method (FEM) simulations of both SECM approach curves and SSV confirm a previously proposed mechanism for the mediated reduction of  $S_2O_8^{2-}$  using Ru(NH<sub>3</sub>) $_6^{3+/2+}$  redox couple. Our results provide a lower limit for dissociation rate constant of  $S_2O_8^{3-}$  (~ 1 × 10<sup>6</sup> s<sup>-1</sup>), as well as the

rate constants for electron transfer between  $SO_4^{\bullet-}$  and  $Ru(NH_3)_6^{2+}$  ( $\sim 1 \times 10^9~M^{-1}s^{-1}$ ) and between  $S_2O_8^{2-}$  and  $Ru(NH_3)_6^{2+}$  ( $\sim 7 \times 10^5~M^{-1}s^{-1}$ ).

# Introduction

Peroxydisulfate  $(S_2O_8^{2-})$  is an oxidizing reagent widely used in industrial processes, such as in the etching of printed circuit boards<sup>1</sup> and water remediation,<sup>2</sup> due to its oxidizing properties, low cost, and ease of handling. Cleavage of the peroxo bond at elevated temperatures or using light, also referred to as  $S_2O_8^{2-}$  activation,<sup>3,4</sup> results in the formation of the sulfate radical anion  $(SO_4^{--})$ , which has a standard reduction potential  $(E^0)$  of ~ 2.2 V vs. Ag/AgCl.<sup>5</sup> The resulting  $SO_4^{--}$  is capable of abstracting an electron or a hydrogen atom from molecules to form  $SO_4^{2-}$  or  $HSO_4^{--}$ , respectively.<sup>2</sup> The ability of  $SO_4^{--}$  to abstract a hydrogen atom is leveraged frequently in organic synthesis for C-H activation.<sup>6-8</sup> For instance, McMillan and coworkers carried out  $\alpha$ -arylation of ethers using photochemical reduction of  $S_2O_8^{2--9}$ 

Recently, we reported the selective oxidation of alcohols to the corresponding aldehydes/ketones (pH < 7) and carboxylic acids (pH > 7) via the electrocatalytic reduction of  $S_2O_8^{2-}$  to  $S_2O_8^{3-}$  using electrogenerated Ru(NH<sub>3</sub>)6<sup>2+</sup>.<sup>10</sup> Our prior studies suggested an eight-step mechanism for the overall alcohol oxidation, with the first five steps, shown below as eqs. 1-5, involving the generation of  $SO_4^{-}$  (eqs. 1-3) followed by its reaction either with Ru(NH<sub>3</sub>)6<sup>2+</sup> (eq. 4) or by direct reduction at the electrode (eq. 5).<sup>10</sup> Eqs. 4 and 5 represent *quenching* reactions, preventing  $SO_4^{-}$  from participating in the intended oxidation of the alcohol substrate. Cyclic voltammetry (CV) studies performed using glassy carbon macroelectrodes, along with finite-difference simulations, were employed to estimate the rate constants of eq. 2 as ~ 2 × 10<sup>5</sup> M<sup>-1</sup>s<sup>-1</sup> and provided lower limits for eq. 3 (> 1 × 10<sup>6</sup> s<sup>-1</sup>), and eq. 4 (> 1 × 10<sup>7</sup> M<sup>-1</sup>s<sup>-1</sup>).<sup>10</sup> Density functional

theory (DFT) and molecular dynamics computational analysis, however, suggest that  $S_2O_8^{3-1}$  fragmentation occurs on time scales of  $\sim 10^{-12}$  s.<sup>10</sup> Similarly, the free energy change for the homogeneous reduction of  $SO_4^{-1}$  by  $Ru(NH_3)_6^{2+}$ , based on  $E^0$  values of eqs. 1 and 5,  $\Delta G \sim -2.4$  eV, would suggest that this single electron-transfer reaction should occur at a diffusion-controlled rate. Thus, the rate constants of eqs. 3 and 4 should be significantly higher than the lower limits previously reported based on CV analysis.

$$Ru(NH_3)_6^{3+} + e^- \rightleftharpoons Ru(NH_3)_6^{2+}$$
  $E^{0'} = -0.12 \text{ V vs. Ag/AgCl}$  (1)

$$Ru(NH_3)_6^{2+} + S_2O_8^{2-} \rightleftharpoons Ru(NH_3)_6^{3+} + S_2O_8^{3-}$$
  $k_2 = 2.0 \times 10^5 \text{ M}^{-1}\text{s}^{-1}$  (2)

$$S_2O_8^{3-} \rightleftharpoons SO_4^{2-} + SO_4^{-}$$
  $k_3 > 1 \times 10^6 \text{ s}^{-1}$  (3)

$$Ru(NH_3)_6^{2+} + SO_4^{--} \rightleftharpoons Ru(NH_3)_6^{3+} + SO_4^{2-}$$
  $k_4 > 1 \times 10^7 \text{ M}^{-1}\text{s}^{-1}$  (4)

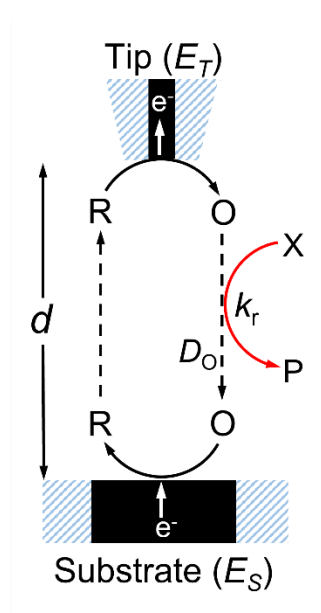
$$SO_4^- + e^- \rightleftharpoons SO_4^{2-}$$
  $E^0 = 2.2 \text{ V vs. Ag/AgCl}$  (5)

Reactions of thermally or photochemically generated SO<sub>4</sub><sup>--</sup> with other species are generally very rapid and have been traditionally investigated using spectroscopic methods. <sup>11,12</sup> The kinetics of rapid homogeneous reactions that follow an initial electron-transfer step, e.g., the oxidation of Ru(NH<sub>3</sub>)<sub>6</sub><sup>2+</sup> by S<sub>2</sub>O<sub>8</sub><sup>2-</sup> (eq. 2), can be investigated using a variety of electrochemical methods, such as fast-scan CV (FSCV)<sup>13</sup> and scanning electrochemical microscopy (SECM). <sup>14</sup> Analysis of data obtained from time-dependent methods, e.g. FSCV, is complicated due to large contributions to the current from capacitive charging and adsorbed species. As a result, SECM analysis, which is generally based on steady-state current-potential (*i-E*) measurements, has been increasingly employed to measure the kinetics of fast electrochemical reactions. <sup>15-17</sup> For instance, Bard and coworkers investigated the rate constants of elementary steps involved in the electrocoxidation of

oxalate and measured the lifetime of transient species  $CO_2^{\bullet-}$  (10 ns) and  $C_2O_4^{\bullet-}$  (1.3 µs) in *N,N*-dimethylformamide.<sup>18,19</sup> In a more recent study, Rodríguez-López, et al. employed SECM in tandem with electrogenrated chemiluminescence to accurately measure ion annhilation rate constant (k<sub>ann</sub>) in reaction consist of Rubrene and [Ru(bpy)<sub>3</sub>]<sup>2+</sup> as k<sub>an</sub> > 1×10<sup>7</sup> M<sup>-1</sup> s<sup>-1</sup>.<sup>20</sup>

The principles of SECM instrumentation and the electrochemical measurements necessary for kinetic investigations are described in detail elsewhere. Briefly, SECM comprises two electrodes, oriented with their active surfaces parallel to each other. Frequently, a disk-shaped metal tip (radius <  $10 \mu m$ ), referred to as an ultramicroelectrode (UME), is used in conjunction with a larger substrate electrode. The electrode potentials of the tip and the substrate are independently controlled, while the distance between the two electrodes (d) is actively controlled using piezoelectric positioners, and can be varied from large distances, where the electrodes are non-interacting, to very small separations, where interactions occur by diffusion and reactions of redox molecules electrogenerated at the two electrodes. The resulting tip current ( $i_1$ ) vs. d plot is referred to as an approach curve and can provide direct experimental insights into the mechanism and kinetics of chemical reactions coupled to an electrode reaction.

Scheme 1 shows a simple conceptual example of using SECM to measure the rate of a bimolecular reaction involving species generated at the tip. Here, the electrochemical oxidation of species R, present in the bulk solution, at the tip electrode yields species Q, which undergoes either a second-order reaction,  $Q + X \rightarrow P$ , to form an electro-inactive species P, or diffuses across the tip-substrate gap to be reduced back to R at the substrate.



**Scheme 1.** Simple example of using SECM in positive feedback mode to measure the rate of a bimolecular reaction,  $O + X \rightarrow P$ . For small values of  $k_r$ , the redox species R and O undergo electrochemical oxidation and reduction at the tip and substrate electrodes, respectively, resulting in positive feedback and an increased tip current as the tip-substrate distance, d, is decreased. For large  $k_r$  values, O is consumed by the homogeneous reaction, resulting in decreased feedback. Approach curves  $(i_t \text{ vs. } d)$  are analyzed to determine  $k_r$ .

In the absence of the chemical reaction, the reduction of O at the substrate electrode, held at a potential negative of formal potential,  $E^{0'}$ , of the O/R couple, results in a positive feedback cycle, corresponding to R diffusing back to the tip electrode where it is oxidized back to O, resulting in an increased tip current. In this limiting case of no homogeneous chemical reaction, the tip current increases from a steady-state constant value at large d (corresponding to no feedback between the tip and substrate) to a much larger value at smaller values of d (corresponding to strong feedback). Conversely, if O is consumed by the chemical reaction before it reaches the substrate to be reduced, the amount of positive feedback is reduced when the tip approaches the substrate.

These basic concepts can be made more quantitative by considering the half-life of O associated with its conversion to  $P(\tau_r)$ , and the timescale of diffusion of O from the tip to the substrate  $(\tau_d)$ , as expressed by eqs. 6 and 7, respectively.

$$\tau_{\rm r} = 1/k_{\rm r} C_{\rm O} \tag{6}$$

$$\tau_{\rm d} = d^2/2D_{\rm O} \tag{7}$$

In eqs. 6 and 7,  $D_0$  and  $C_0$  are the diffusion coefficient (D) and concentration of O, respectively, and  $k_r$  is the second-order rate constant for  $O+X\to P$ . The expression for  $\tau_r$ , eq. 6, is approximate and assumes that the initial bulk concentrations of R and X are equal (a condition that is generally not true). A negligible amount of O arrives at the substrate electrode when  $\tau_d \gg \tau_r$  (i.e., large d and/or large  $k_r$ ). With decreasing d or  $k_r$ ,  $\tau_d$  can be comparable to or less than  $\tau_r$ , i.e.,  $\tau_d \le \tau_r$ . Under these conditions, a larger fraction of O survives the crossing of the tip-substrate gap without reaction, resulting in its reduction at the substrate electrode, and subsequent diffusion of R back to the UME tip resulting in positive feedback. Therefore, the substrate electrode approach curve and the collection efficiency (i.e., the ratio of the substrate electrode current to the tip electrode current) as a function of d provides quantitative information about  $k_r$ . Analyses of SECM approach curves to verify a proposed mechanism or to determine reaction rate constants are generally performed by comparing computer simulations based on diffusion and reaction rate expressions to the experimental data. Detailed discussions of using SECM to analyze many different reaction mechanisms can be found in the literature.

When combined, eqs. 6 and 7 suggest that the measurement of very fast kinetics requires very small values of d. For instance, a reaction with  $k_r = 10^9 \,\mathrm{M}^{-1}\mathrm{s}^{-1}$  and  $C_\mathrm{O} \sim C_\mathrm{X} \sim 1 \,\mathrm{mM}$  requires tip-substrate separation on the order of  $d \sim 10$ -100 nm in order to observe the effect of the chemical reaction on the feedback current, assuming a typical value of  $\sim 10^{-5} \,\mathrm{cm}^2/\mathrm{s}$  for  $D_\mathrm{O}$ . This experimental requirement of very small d values is very challenging due to the necessity of fabricating nanotip electrodes that allow the positioning of the tip very close to the substrate.

Herein, we report the use of steady-state voltammetry (SSV) at UMEs and SECM for investigating the mechanism and rates of  $S_2O_8^{2-}$  reduction using the Ru(NH<sub>3</sub>)<sub>6</sub><sup>3+/2+</sup> electrocatalyst system. As discussed above, prior cyclic voltammetry investigations allowed only estimates of the lower limits of the rate constants for  $S_2O_8^{3-}$  dissociation (eq. 3) and the bimolecular electron-transfer reaction between  $SO_4^{-}$  with Ru(NH<sub>3</sub>)<sub>6</sub><sup>2+</sup> (eq. 4). We show that SECM approach curves, obtained using a relatively large tip (3.5- $\mu$ m radius), can be used to measure the electron-transfer rate constant for the reaction between  $SO_4^{-}$  with Ru(NH<sub>3</sub>)<sub>6</sub><sup>2+</sup>, which approaches a diffusion-limited value (~  $10^9$  M<sup>-1</sup>s<sup>-1</sup>), corresponding to one of the fastest bimolecular reactions ever measured using SECM. The ability to measure such fast reactions with a large tip is a somewhat counter-intuitive finding and, as shown below, results from spatial localization of homogeneous electron-transfer reactions near both the tip and substrate electrodes. Finally, we present a straightforward approach to fabricate carbon ultramicroelectrodes (UME) with moderately small insulator-to-electrode radius ratios (referred to as the *RG* ratio in SECM analysis).

#### **Materials and Methods**

Reagents.

The following reagents were used as received: Ag ink (Sigma Aldrich), W rod (diameter = 0.0254 mm, Goodfellow), platinum wire (radius = 25  $\mu$ m, Goodfellow), carbon fiber (radius = 3.5  $\mu$ m, Goodfellow), hexaammineruthenium(III) chloride (Sigma Aldrich, 98%), sodium peroxydisulfate (Fisher Scientific, 98%), potassium chloride (Fisher Scientific, 99%). The capillary glass was purchased from King Precision Glass Inc. (ID = 0.4267  $\pm$  0.0500, OD = 1.00  $\pm$  0.05, and L = 75  $\pm$  3.0 mm) and treated as outlined previously. Aqueous solutions were prepared using Millipore water. An adhesive epoxy (LOCTITE® EA 9340), 3M aluminum oxide Microfinishing/lapping film, and Microcut S polishing cloth (Buehler) were used in C-UME preparation.

#### Electrochemical Instrumentation.

Voltammetric studies were performed using a Biologics Dual Channel SP300 Potentiostat, equipped with a low current amplifier. The SECM measurements were performed using a homebuilt bipotentiostat comprised of a Dagan Chem-Clamp with a preamplifier head-stage (Dagan Corporation, U.S.A).<sup>27</sup> University of Warwick electrochemical scanning probe microscopy software was used to record current–time and current–distance curves.<sup>28</sup> Acquired data were processed with OriginPro 2022 software.

# Fabrication of UME

The C-UMEs used for the SECM experiments were prepared with the four-step process as depicted in Figure S1, adapted in part from the report by Mauzeroll and coworkers.<sup>26</sup> A detailed description of the procedure for preparation of C-UME is presented in the Supporting Information. In summary, the C fiber was inserted into the glass capillary. Next, the C fiber and the glass

capillary were pulled together using a P-2000 Sutter laser puller. Finally, the tapered glass with the enclosed C fiber were subjected to thermal treatment and the follow-up precision polishing to make a flat disk with RG ratio (glass-to-C radius ratio). As shown in Figure 1, this fabrication procedure yields C-UMEs of  $RG \sim 5$  with RG values varied slightly for different electrodes.

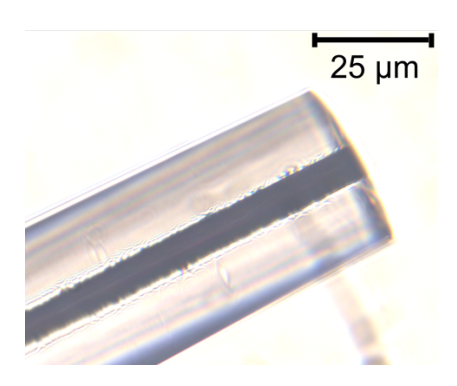


**Figure 1.** Side view of a homemade C-UME obtained with an optical microscope. The RG ratio of the C-UME was estimated as  $\sim 5$ .

Detailed procedures to make C- and Pt-UMEs with large RG ratios (i.e., > 20) for the SSV and SECM measurements are presented in the Supporting Information. Briefly, a  $\sim$  5 mm piece of C or Pt wire was connected to a stiff W rod via Ag ink. Next, the W rod with the electrode material on the leading end was inserted into the glass capillary, one end of which had been previously sealed in an oxyhydrogen torch. Once the electrode material touched the sealed end of the capillary, the assembly was heated in the oxyhydrogen torch to incorporate the electrode material into the glass. Finally, the electrode was polished to expose the electrode material and obtain a flat surface.

Finite Element (FEM) Simulations.

The SSV and SECM simulations were performed using COMSOL Multiphysics® v5.4 software. The Supporting Information provides: a full Comsol simulation report; a simplified representation of the 2-D axisymmetric simulation model; a summary of reaction parameter values; diffusion-reaction equations; initial and boundary conditions; and equations for the currents at the tip and the substrate.

#### **Results and Discussions**

SSV Analysis

Figure 2 shows SSVs recorded using a 3.5- $\mu$ m radius C-UME in an O<sub>2</sub>-free aqueous solution containing 1.0 mM Ru(NH<sub>3</sub>)6<sup>3+</sup> and 0.1 M KCl. In the absence of S<sub>2</sub>O<sub>8</sub><sup>2-</sup>, the voltammogram reaches a steady-state diffusion-limited current of ~ -1.1 nA at potentials more negative than -0.30 V vs. Ag/AgCl. With the addition of increasing amounts of S<sub>2</sub>O<sub>8</sub><sup>2-</sup> (corresponding to S<sub>2</sub>O<sub>8</sub><sup>2-</sup> concentrations between 0.60 to 2.4 mM), the voltammetric current increases steadily, a consequence of the electrocatalytic homogeneous reduction of S<sub>2</sub>O<sub>8</sub><sup>2-</sup> by Ru(NH<sub>3</sub>)6<sup>2+</sup> (eq. 2), which regenerates Ru(NH<sub>3</sub>)6<sup>3+</sup>. Additionally, the dissociation of S<sub>2</sub>O<sub>8</sub><sup>3--</sup> yields SO<sub>4</sub><sup>--</sup>, which is also either directly reduced to SO<sub>4</sub><sup>2-</sup> at the electrode (eq. 5) or reduced through its homogeneous reaction with Ru(NH<sub>3</sub>)6<sup>2+</sup> to yield Ru(NH<sub>3</sub>)6<sup>3+</sup> (eq. 4) that is then reduced at the electrode (eq. 1). Thus, the combination of eqs. 1 and 4 (mediated reduction of SO<sub>4</sub><sup>--</sup> pathway) is equivalent to eq. 5 (direct reduction of SO<sub>4</sub><sup>--</sup> pathway), both resulting in a second electron transferred from the electrode to yield SO<sub>4</sub><sup>2-</sup>. The overall reaction for the mediated reduction of S<sub>2</sub>O<sub>8</sub><sup>2-</sup>, eq. (8), is obtained by combining eqs. 1, 2, 3, and 5 (direct reduction of SO<sub>4</sub><sup>--</sup> pathway).

$$S_2O_8^{2-} + 2e \rightarrow 2 SO_4^{2-}$$
 (8)

The SSVs in the presence of  $S_2O_8^{2-}$ , Figure 2, show several non-ideal behaviors: (i) a prewave at the foot of the main wave, (ii) a small hysteresis between the forward and reverse scan, and (iii) a sloping limiting current that becomes more apparent at high  $S_2O_8^{2-}$  concentrations. We believe that at least a partial explanation for these non-idealities is either the adsorption of  $S_2O_8^{2-}$ , the onset of direct  $S_2O_8^{2-}$  reduction at the C-UME electrode, and/or ion-pairing between  $Ru(NH_3)6^{3+}$  (and/or  $Ru(NH_3)6^{2+}$ ) with  $S_2O_8^{2-}$ . While we have not systematically investigated any of these possibilities, we note previous reports of ion-pairing of  $Ru(NH_3)6^{3+}$  with  $SO_4^{2-}$  in aqueous solutions,<sup>29</sup> and ion-pairing of  $Ru(bpy)_3^{2+}$  with  $S_2O_8^{2-}$  (where bpy = 2,2'-bipyridine) in mixed  $H_2O$ /acetonitrile solutions.<sup>30</sup> Additionally, the SSV response for the direct reduction of  $S_2O_8^{2-}$  at the C-UME, shown in the Supporting Information, indicates that  $S_2O_8^{2-}$  reduction, which is kinetically slow at C, commences at about -0.45 V vs Ag/AgCl. While these non-ideal behaviors limit our analysis of the SSV response, the increase in current upon addition of  $S_2O_8^{2-}$  to the solution is clearly dominated by the electrocatalytic reduction of  $S_2O_8^{2-}$  by  $Ru(NH_3)_6^{3+}$ , as discussed above.

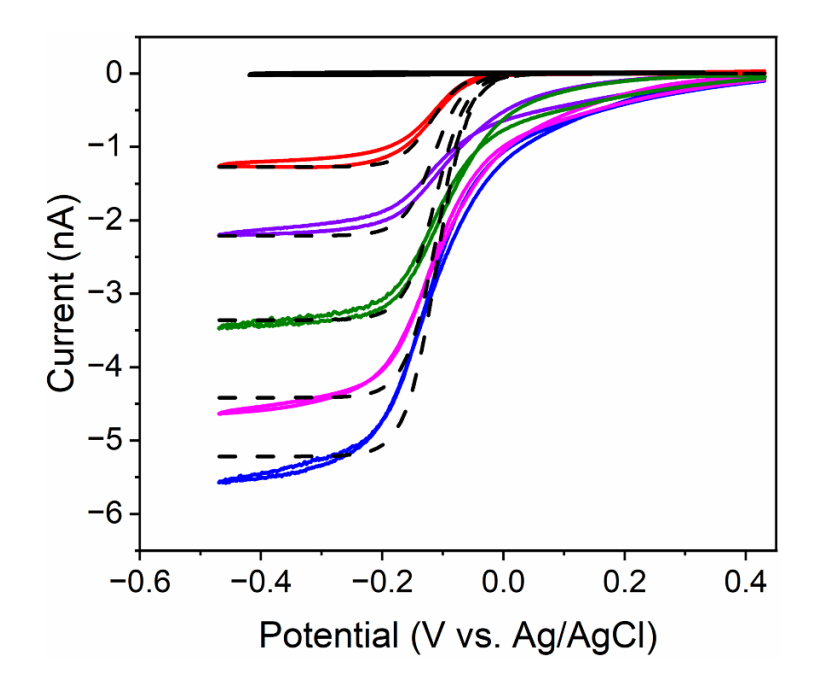


**Figure 2**. Experimental (solid lines) and simulated (dashed lines) voltammograms for aqueous solutions containing 0.1 M KCl (black), 1.0 mM Ru(NH<sub>3</sub>)<sub>6</sub><sup>3+</sup> and 0.1 M KCl (red), and 1.0 mM Ru(NH<sub>3</sub>)<sub>6</sub><sup>3+</sup> with 0.1 M KCl and  $S_2O_8^{2-}$  at 0.60 (purple), 1.2 (green), 1.8 (magenta), and 2.4 mM (blue). All voltammograms were recorded at v = 5 mV/s with 3.5- $\mu$ m radius C-UME working electrode in an O<sub>2</sub>-free aqueous solution. The potential of the working electrode was swept from 0.4 V to -0.5 V and back to 0.4 V.

The SSV responses of the C-UME in the absence and presence of  $S_2O_8^{2-}$  were simulated with the FEM method. Details of FEM simulations including major assumptions, diffusion coefficient of various species (*D*), heterogeneous electron transfer rate constants, and standard reduction potentials ( $E^0$ ) are reported in the Supporting Information. Moreover, Table S1 and S2 provides a complete list of thermodynamic and kinetic parameters used in the simulation.

Best fits of simulations to the experimental SSVs using the above-mentioned parameters were obtained by adjusting the rate constant,  $k_2$ , for the homogeneous electron transfer between  $Ru(NH_3)_6^{2+}$  and  $S_2O_8^{2-}$ , eq. 2. The dissociation rate constant of  $S_2O_8^{3-}$ ,  $k_3$ , was assumed to be  $1 \times 10^{10}$  s<sup>-1</sup>, consistent with theoretical estimates. The homogeneous reaction between  $SO_4^{-}$  and  $Ru(NH_3)_6^{2+}$  (eq. 4) was assumed to be diffusion-controlled; hence a rate constant of  $1 \times 10^{10}$  M<sup>-</sup>

 $^{1}$ s $^{-1}$  was used for  $k_4$ . Our simulations only approximated the observed SSV response due to the non-idealities in the experimental curves, as discussed above. Additionally, we found that the set of voltammograms in Figure 2 acquired at different  $S_2O_8^{2-}$  concentrations (0.60 to 2.4 mM) could not be fit by a unique value of  $k_2$  (see Table S2). Rather, the best fits over this concentration range required varying  $k_2$  from  $1.5 \times 10^5$  to  $6.5 \times 10^5$  M $^{-1}$ s $^{-1}$  with increasing  $S_2O_8^{2-}$  concentration.

In a previous report, we showed that the simulations of the cyclic voltammetric (CV) response for the same system, but using a large glassy carbon electrode (radius = 1.49 mm), were in near-perfect agreement with experimental CVs obtained in solutions containing 1.0 mM Ru(NH<sub>3</sub>)<sub>6</sub><sup>3+</sup>, 0.1 M NaSO<sub>4</sub>, and S<sub>2</sub>O<sub>8</sub><sup>2-</sup> (2 to 8 mM).<sup>10</sup> In addition to the electrode material and size, the only difference between the present and prior experiments is the choice of supporting electrolyte, KCl vs. Na<sub>2</sub>SO<sub>4</sub>, respectively. A single value of  $k_2 = 2.0 \times 10^5$  M<sup>-1</sup>s<sup>-1</sup> for the reaction between Ru(NH<sub>3</sub>)<sub>6</sub><sup>2+</sup> and S<sub>2</sub>O<sub>8</sub><sup>2-</sup> (eq. 2) was found to yield good fits to the prior CV results, independent of S<sub>2</sub>O<sub>8</sub><sup>2-</sup> concentration, in reasonable agreement with values listed in Table S2. However, we do not have an explanation for why  $k_2$  in the SSV experiments appears to increase as a function of S<sub>2</sub>O<sub>8</sub><sup>2-</sup> concentration. As shown below, with increasing concentration of S<sub>2</sub>O<sub>8</sub><sup>2-</sup>, a slightly larger  $k_2$  value is also needed to simulate SECM approach curves obtained in 0.1 M KCl solutions containing 1.0 mM Ru(NH<sub>3</sub>)<sub>6</sub><sup>3+</sup>, consistent with the SSV findings.

# SECM Analysis

In order to provide an initial validation of the SECM methodology, approach curves were obtained in an O<sub>2</sub>-free solution containing 1.0 mM Ru(NH<sub>3</sub>) $_6$ <sup>3+</sup> and 0.1 M KCl. The potential of the C tip and Pt substrate electrodes were set at -0.4 and 0.4 V vs Ag/AgCl, respectively, to reduce Ru(NH<sub>3</sub>) $_6$ <sup>3+</sup> and oxidize Ru(NH<sub>3</sub>) $_6$ <sup>2+</sup> at their diffusion-controlled rates. In SECM analysis,

approach curves showing the dependencies of the tip and substrate currents ( $i_1$  and  $i_s$ ) on the distance between the tip and substrate, d, are generally plotted in terms of a normalized distance, L = d/a, where a is the tip radius. Figure 3 shows typical  $i_t$ -L and  $i_s$ -L curves (black) recorded in the absence of  $S_2O_8^{2-}$ . These curves correspond to the classical positive feedback mechanism between the two electrodes, as depicted in Scheme 2A. At large values of L,  $i_t$  approaches the value of the diffusion-limited current observed in SSV (i.e.,  $\sim -1$  nA, Figure 2), while  $i_s$  falls to zero. Conversely, as the tip approaches the substrate (L < 2.5), both  $i_t$  and  $i_s$  rapidly increase indicating the onset of strong positive feedback. FEM simulations of the approach curves presented in the Supporting Information are in good agreement with experimental curves for this simple experiment, and demonstrate that, as expected, essentially 100 % of the Ru(NH<sub>3</sub>)<sub>6</sub><sup>2+</sup> generated at the C tip is oxidized at the Pt substrate when L < 2.5 (i.e.,  $d < 9 \mu m$ ).

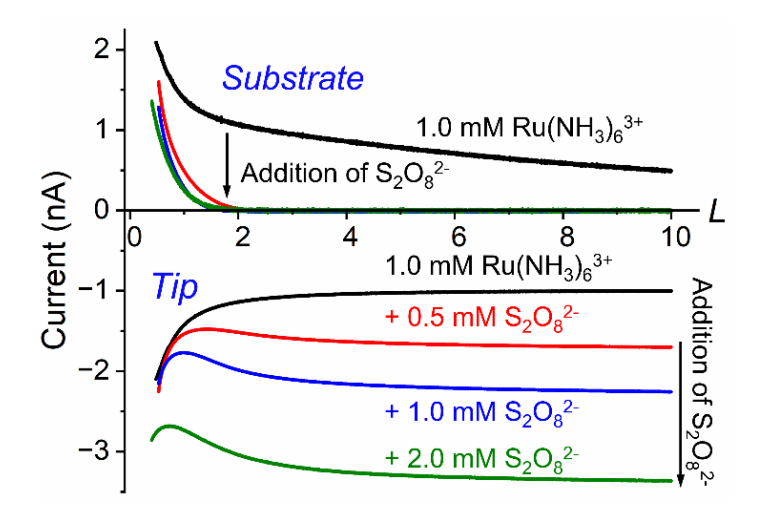


**Figure 3**. Experimental approach curve for 1.0 mM Ru(NH<sub>3</sub>)<sub>6</sub><sup>3+</sup> in the absence of S<sub>2</sub>O<sub>8</sub><sup>2-</sup> (black) and the presence of 0.50 (red), 1.0 (blue), and 2.0 mM S<sub>2</sub>O<sub>8</sub><sup>2-</sup> (green). Approach curves were recorded using a 3.5-μm radius C-UME tip electrode (RG ~ 5) and a 25-μm radius Pt-UME substrate electrode (RG = 20). All measurements were made in an O<sub>2</sub>-free aqueous solution containing 0.1 M KCl at pH = 6.50. Positive current at the substrate ( $i_s$ ) corresponds to a net oxidation; negative currents,  $i_t$ , at the tip correspond to a net reduction.

SECM approach curves obtained in solutions containing Ru(NH<sub>3</sub>)<sub>6</sub><sup>3+</sup>, S<sub>2</sub>O<sub>8</sub><sup>2-</sup>, and KCl are significantly more complex than in solutions containing only Ru(NH<sub>3</sub>)<sub>6</sub><sup>3+</sup> and KCl, due to reactions involved in the electrocatalytic reduction of S<sub>2</sub>O<sub>8</sub><sup>2-</sup>. Scheme 2B depicts what we believe are the important heterogeneous and homogeneous reactions occurring between the tip and substrate electrodes, following the initial reduction of Ru(NH<sub>3</sub>)<sub>6</sub><sup>3+</sup> at the tip electrode. As before, the tip and substrate electrodes are held at potentials corresponding, respectively, to the diffusion-limited reduction of Ru(NH<sub>3</sub>) $_6^{3+}$  (-0.4 V) and oxidation of Ru(NH<sub>3</sub>) $_6^{2+}$  (0.4 V). In addition to these reactions, SO<sub>4</sub> can be reduced at either the tip or the substrate, since the reduction potential for the SO<sub>4</sub>\*-/SO<sub>4</sub><sup>2-</sup> couple, 2.21 V, is very positive of either tip or substrate electrode potential. Thus, upon formation and dissociation of S<sub>2</sub>O<sub>8</sub><sup>3</sup>·- to yield SO<sub>4</sub>·-, both Ru(NH<sub>3</sub>)<sub>6</sub><sup>3+</sup> and SO<sub>4</sub>·- are reduced at the C tip. At the Pt substrate,  $Ru(NH_3)_6^{2+}$  is oxidized while  $SO_4^{\bullet-}$  is also reduced. As noted above in the discussion of the SSV data, Ru(NH<sub>3</sub>)<sub>6</sub><sup>2+</sup> is homogeneously oxidized back to Ru(NH<sub>3</sub>)<sub>6</sub><sup>3+</sup> through its reaction with either S<sub>2</sub>O<sub>8</sub><sup>2-</sup> or SO<sub>4</sub>. A key objective of the SECM measurement is the determination of the rate constant for the reaction of  $Ru(NH_3)_6^{2+}$  with  $SO_4^{\bullet-}$  (i.e., eq. 4). As before, the dimerization of  $SO_4$  to yield  $S_2O_8^{2-}$  was not included in the simulation analysis due to its negligible concentration in the gap region (see Supporting Information).

The approach curves shown in Figure 3 for solutions containing both  $Ru(NH_3)6^{3+}$  and  $S_2O_8^{2-}$  can be summarized as follows:

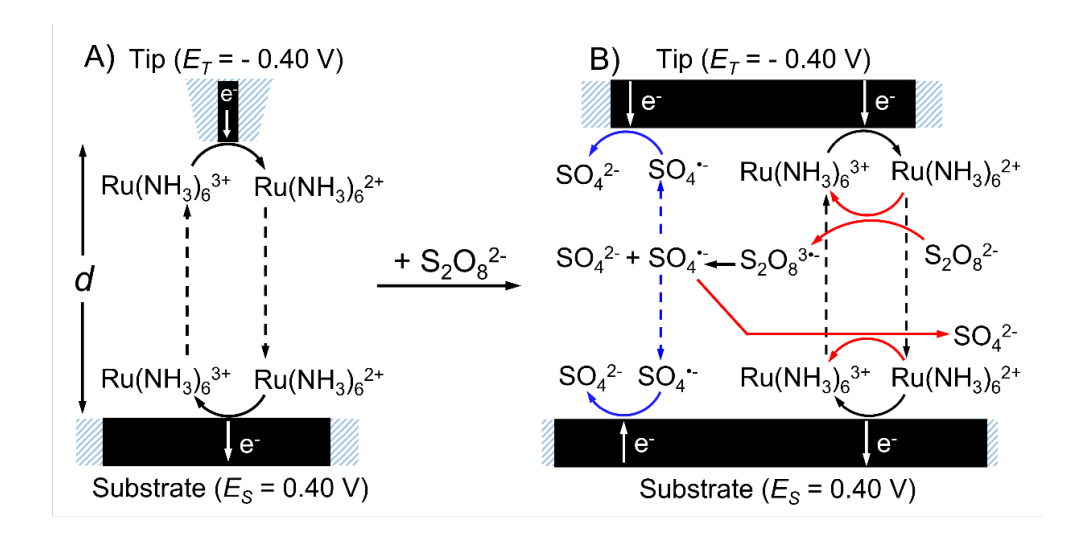
# Substrate:

• At large gap separations, 2 < L < 10 (7.0  $\mu m < d < 35 \mu m$ ),  $i_s$  decreases to the baseline, indicating that all Ru(NH<sub>3</sub>)<sub>6</sub><sup>2+</sup> generated at the tip electrode reacts with S<sub>2</sub>O<sub>8</sub><sup>2-</sup> or SO<sub>4</sub><sup>--</sup>

- before it reaches the substrate electrode, and/or that the anodic current due to oxidation of  $Ru(NH_3)_6^{2+}$  is precisely canceled out by the cathodic current due to reduction of  $SO_4^{\bullet-}$ .
- At small gap separations, L < 2 ( $d < 7.0 \mu m$ ),  $i_s$  increases rapidly with decreasing L as  $Ru(NH_3)_6^{2+}$  starts to arrive at the substrate electrode resulting in positive feedback.
- As shown in Figure 3, the  $i_s$  L curves are essentially independent of  $S_2O_8^{2-}$  concentration.

# Tip:

- At large gap separations, 3 < L < 10 (i.e.,  $10.5 \mu m < d < 35 \mu m$ ),  $i_t$  remains essentially constant, confirming that the substrate electrode has no influence on the rate of Ru(NH<sub>3</sub>)<sub>6</sub><sup>3+</sup> reduction and the following homogeneous chemical reactions. The magnitude of  $i_t$  increases with increasing S<sub>2</sub>O<sub>8</sub><sup>2-</sup> due to the electrocatalytic reduction of S<sub>2</sub>O<sub>8</sub><sup>2-</sup>, analogous to the mechanism offered for the SSV response.
- At intermediate gap separations, 1.5 < L < 3 (5.25  $\mu m < d < 10.5 \mu m$ ),  $i_t$  decreases with decreasing L, due to the reduction of mass transport of  $S_2O_8^{2-}$  from the bulk solution into the gap region.
- At small gap separations, L < 1.5 (d < 5.25 µm),  $i_t$  increases rapidly with decreasing L as  $Ru(NH_3)_6^{2+}$  starts to arrive at the substrate electrode resulting in positive feedback to the tip.



**Scheme 2**. Electrochemical and chemical reactions occurring in the gap region between the tip and the substrate electrode in the (A) absence and (B) presence of the  $S_2O_8^{2-}$ . The dashed lines represent diffusion.

The enhancement of  $i_t$  with increasing  $S_2O_8^{2-}$  concentration for 2 < L < 10 (*i.e.*, red, blue, and green trace in Figure 3) is attributed to the increasingly rapid regeneration of Ru(NH<sub>3</sub>)<sub>6</sub><sup>3+</sup> by the reaction of Ru(NH<sub>3</sub>)<sub>6</sub><sup>2+</sup> with  $S_2O_8^{2-}$  and  $SO_4^{--}$  (*i.e.*, eqs. 2 and 4). FEM simulations were used to determine the value of  $k_2$  from the tip and substrate approach curves. In these simulations, the dissociation of  $S_2O_8^{3--}$  yielding  $SO_4^{--}$  was assumed to be very fast ( $k_3 = 10^{10} \text{ s}^{-1}$ ). Also, the homogeneous electron-transfer reaction between  $SO_4^{--}$  and Ru(NH<sub>3</sub>)<sub>6</sub><sup>2+</sup> was assumed to be diffusion-controlled ( $k_4 = 10^{10} \text{ M}^{-1}\text{s}^{-1}$ ). Small variations of these values had no effect on the simulated results. As shown in Figure 4,  $k_2$  was determined as  $\sim 1 \times 10^6 \text{ M}^{-1}\text{s}^{-1}$  for a solution containing 2.0 mM  $S_2O_8^{2-}$  and 1.0 mM Ru(NH<sub>3</sub>)<sub>6</sub><sup>3+</sup>. Similarly, values for  $k_2$  in solutions containing 0.50 mM  $S_2O_8^{2-}$  and 1.0 mM  $S_2O_8^{2-}$  were determined to be  $\sim 5 \times 10^5$  and  $\sim 6 \times 10^5$  M<sup>-1</sup>s<sup>-1</sup>, respectively (Supporting Information). In conclusion,  $k_2$  determined by SECM increased by approximately a factor of 2x for  $S_2O_8^{2-}$  concentrations between 0.5 and 2 mM, with an average value of 7.0 ( $\pm$  2.4)  $\times$  10<sup>5</sup> M<sup>-1</sup>s<sup>-1</sup>, in reasonable agreement with values determined by SSV (Table S2), but somewhat higher than previously obtained using CV ( $\sim$  2  $\times$  10<sup>5</sup> M<sup>-1</sup>s<sup>-1</sup>).

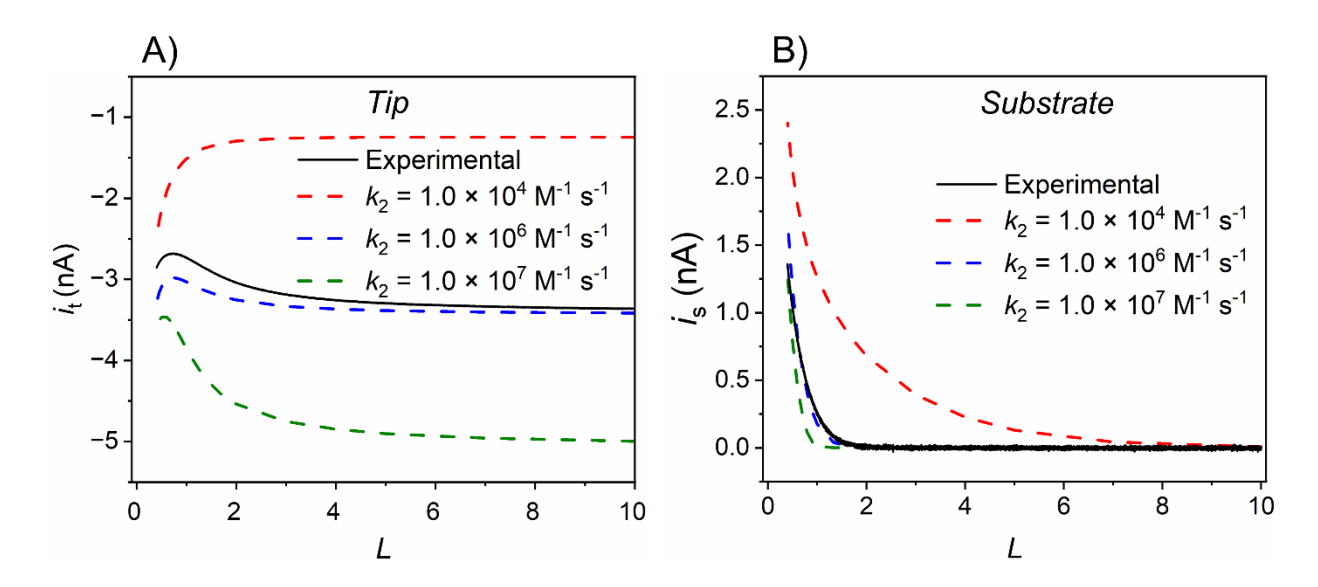


**Figure 4.** Effect of  $k_2$  on the (A) tip and the (B) substrate current. Solid black lines show the experimental approach curves for 1.0 mM Ru(NH<sub>3</sub>)<sub>6</sub><sup>3+</sup> and 2.0 mM S<sub>2</sub>O<sub>8</sub><sup>2-</sup>, and dashed colored lines represent the FEM simulations using  $k_2$  values of 1.0 × 10<sup>4</sup> M<sup>-1</sup>s<sup>-1</sup> (red), 1.0 × 10<sup>6</sup> M<sup>-1</sup>s<sup>-1</sup> (blue), and 1.0 × 10<sup>7</sup> M<sup>-1</sup>s<sup>-1</sup> (green). Approach curves were recorded using a 3.5-μm radius C-UME tip electrode (RG ~ 5) and a 25-μm radius (RG = 20) Pt-UME substrate electrode in an O<sub>2</sub>-free aqueous solution containing 0.1 M KCl (pH = 6.50). All simulations were carried out using  $k_3 = 1.0 \times 10^{10}$  s<sup>-1</sup>,  $k_4 = 1.0 \times 10^{10}$  M<sup>-1</sup>s<sup>-1</sup>.

The decrease of  $i_t$  between 1.5 < L < 3, Figure 4A, is the result of hindered mass transport of  $S_2O_8^{2-}$  and  $Ru(NH_3)_6^{3+}$  into the gap region caused by the proximity of the substrate electrode to the tip. This argument is supported by FEM simulations, discussed in detail in the Supporting Information. Finally, further decreasing L below 1.5 causes  $i_t$  to increase, a consequence of simple redox cycling of  $Ru(NH_3)_6^{3+/2+}$  between the tip and the substrate electrode, Figure 4A.

As indicated in Scheme 2B,  $i_s$  is the sum of the current due to oxidation of Ru(NH<sub>3</sub>)<sub>6</sub><sup>2+</sup> and the reduction of SO<sub>4</sub>\*-. As shown in 4B,  $i_s$  decreases to the zero current baseline level for L > 2 in the presence of S<sub>2</sub>O<sub>8</sub><sup>2-</sup>. Two possible explanations for this decrease are: i) generation of equal currents at the substrate with opposite polarity arising from eq. 5 and eq. 1, or ii) reaction of SO<sub>4</sub>\*- and Ru(NH<sub>3</sub>)<sub>6</sub><sup>2+</sup> (eq. 4) in the gap region, resulting in negligible amounts of SO<sub>4</sub>\*- and Ru(NH<sub>3</sub>)<sub>6</sub><sup>2+</sup> being transported to the substrate electrode. Simulated concentration profiles of Ru(NH<sub>3</sub>)<sub>6</sub><sup>3+</sup>,

Ru(NH<sub>3</sub>) $_6^{2+}$ , S<sub>2</sub>O<sub>8</sub> $_6^{2-}$ , and SO<sub>4</sub> $_6^{--}$  are shown in Figure 5 for L=10, 1.5, and 0.35. At large and moderate values of L, the simulations indicate that SO<sub>4</sub> $_6^{--}$  and Ru(NH<sub>3</sub>) $_6^{2+}$  react within the gap, before reaching the substrate electrode. The concentrations of both species are negligibly small in the proximity of the substrate, resulting in zero current. Conversely, for L<2 (Figure 5), the decreased flux of S<sub>2</sub>O<sub>8</sub> $_6^{2-}$  into the gap reduces the amount of SO<sub>4</sub> $_6^{--}$  generated by homogeneous reactions, allowing Ru(NH<sub>3</sub>) $_6^{2+}$  to reach the substrate, resulting in a significant anodic  $i_8$ , and the corresponding feedback to the tip. Inspection of the concentration gradients of Ru(NH<sub>3</sub>) $_6^{2+}$  and Ru(NH<sub>3</sub>) $_6^{3+}$  in Part E of Figure 5, corresponding to L=0.35, shows that the flux of Ru(NH<sub>3</sub>) $_6^{2+}$  at the substrate is just slightly lower than that of Ru(NH<sub>3</sub>) $_6^{3+}$  at the tip.

The concentration profiles for  $SO_4^{\bullet-}$  are shown for L=10, 1.5, and 0.35 on an expanded scale in parts B, D, and F in Figure 5. Noting the change in the concentration scale ( $\mu$ M instead of mM), it is clear that the concentration of  $SO_4^{\bullet-}$  is vanishingly small at all gap distances. This appears to be a consequence of the heterogeneous reduction of  $SO_4^{\bullet-}$  at both electrodes, as well as its reduction by  $Ru(NH_3)_6^{2+}$  in the solution between the tip and gap. The low concentration of  $SO_4^{\bullet-}$  for all values of L clearly justifies ignoring the second-order dimerization of  $SO_4^{\bullet-}$  to  $S_2O_8^{2-}$ , as previously noted.

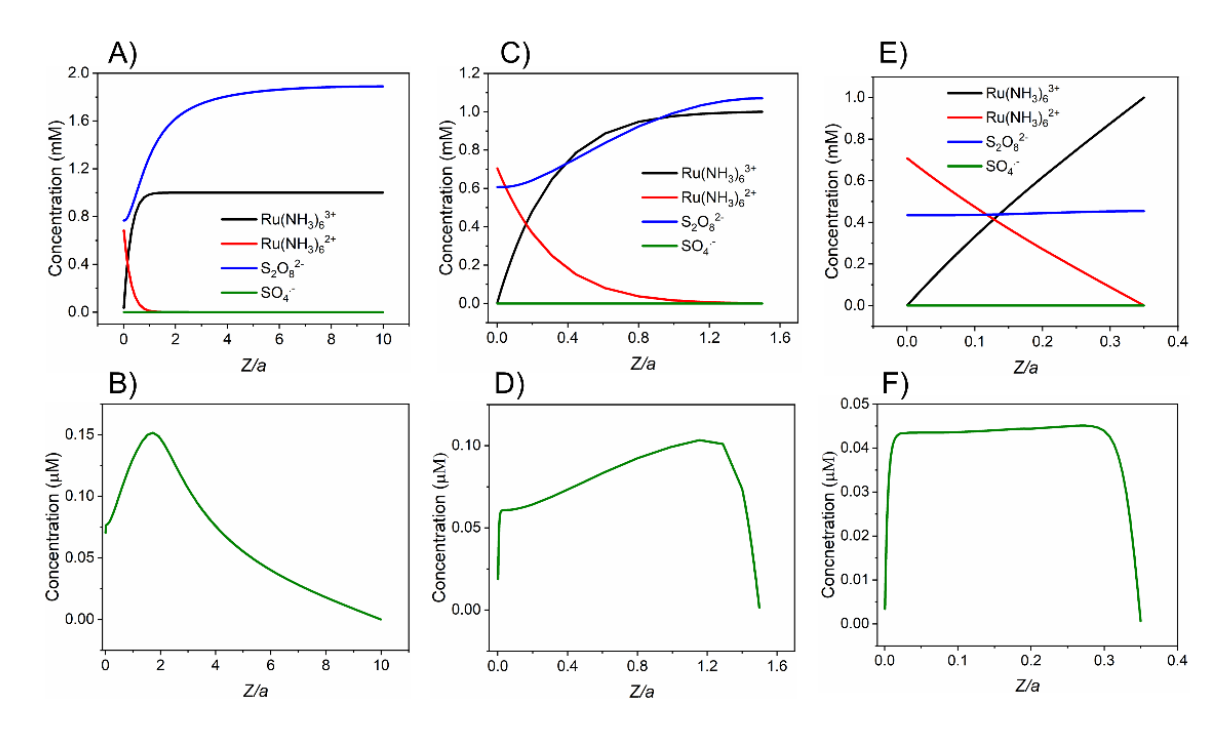


**Figure 5**. Concentration profiles of Ru(NH<sub>3</sub>) $_6^{3+}$  (black), Ru(NH<sub>3</sub>) $_6^{2+}$  (red), S<sub>2</sub>O<sub>8</sub><sup>2-</sup> (blue), and SO<sub>4</sub><sup>--</sup> (green) for L = 10 (A, B), 1.5 (C, D) and 0.35 (E, F). Concentration profiles were extracted from FEM simulations for an aqueous solution containing 1.0 mM Ru(NH<sub>3</sub>) $_6^{3+}$  and 2.0 mM S<sub>2</sub>O<sub>8</sub><sup>2-</sup> with  $k_2 = 1.0 \times 10^6$  M<sup>-1</sup>s<sup>-1</sup>,  $k_3 = 1.0 \times 10^{10}$  s<sup>-1</sup>, and  $k_4 = 1.0 \times 10^{10}$  M<sup>-1</sup>s<sup>-1</sup> with a 3.5-μm radius (RG = 5) C-UME tip electrode and 25-μm radius (RG = 20) Pt-UME substrate electrode.

FEM simulations were also used to determine the rate,  $k_4$ , for the electron-transfer reaction between Ru(NH<sub>3</sub>)<sub>6</sub><sup>2+</sup> and SO<sub>4</sub>\*-. Figure 6 shows simulated approach curves with various  $k_4$  values, while the  $k_2$  and  $k_3$  were held constant at  $1.0 \times 10^6$  M<sup>-1</sup>s<sup>-1</sup> and  $1.0 \times 10^{10}$  s<sup>-1</sup>, respectively. The simulated approach curves for  $i_t$  and  $i_s$  converged to the experimental data with increasing  $k_4$  values and remained sensitive to  $k_4$  for values approaching up to  $1 \times 10^9$  M<sup>-1</sup>s<sup>-1</sup>, which is two orders of magnitude higher than our previous lower limit determined by CV using a glassy carbon macroelectrode. We conclude from the SECM data that  $k_4$  is greater than or equal to  $\sim 1 \times 10^9$  M<sup>-1</sup>s<sup>-1</sup>.

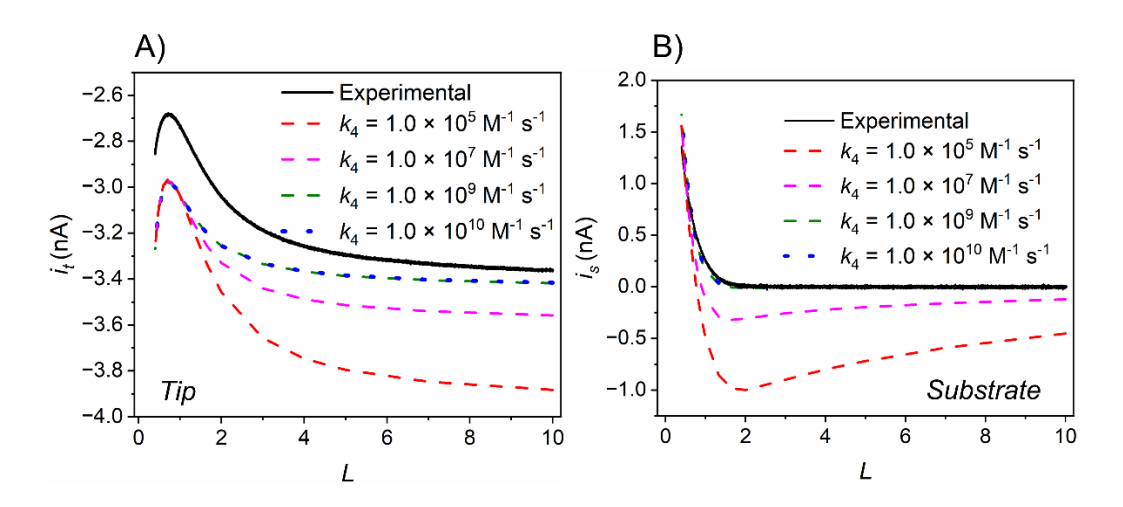


**Figure 6.** Effect of the  $k_4$  on the (A) tip and (B) substrate current. The solid black line shows the experimental approach curve for 1.0 mM Ru(NH<sub>3</sub>)<sub>6</sub><sup>3+</sup> and 2.0 mM S<sub>2</sub>O<sub>8</sub><sup>2-</sup>, and colored lines represent FEM simulation with  $k_4$  values of 1.0 × 10<sup>5</sup> M<sup>-1</sup>s<sup>-1</sup> (dashed red), 1.0 × 10<sup>7</sup> M<sup>-1</sup>s<sup>-1</sup> (dashed magenta), 1.0 × 10<sup>9</sup> M<sup>-1</sup>s<sup>-1</sup> (dashed green), and 1.0 × 10<sup>10</sup> M<sup>-1</sup>s<sup>-1</sup> (dotted blue). Approach curves were recorded using a 3.5-μm radius C-UME tip electrode (RG ~ 5) and a 25-μm radius Pt-UME substrate electrode (RG = 20) in an O<sub>2</sub>-free aqueous solution containing 0.1 M KCl (pH = 6.50). All simulations were carried out using  $k_2$  = 1.0 ×10<sup>6</sup> M<sup>-1</sup>s<sup>-1</sup> and  $k_3$  = 1.0 ×10<sup>10</sup> M<sup>-1</sup>s<sup>-1</sup>.

Finally, the approach curves of both the tip and the substrate electrode were simulated via FEM simulations using the rate constants determined by the above SECM measurements and compared to the experimental curves for 1.0 mM Ru(NH<sub>3</sub>)<sub>6</sub><sup>3+</sup> and S<sub>2</sub>O<sub>8</sub><sup>2-</sup> concentrations of 0.50, 1.0, and 2.0 mM. It is clear from the results shown in Figure 7A-C that the simulated approach curves for  $i_t$  and  $i_s$  are in reasonably good agreement with the experimental curves, supporting the accuracy of the values of  $k_2$ ,  $k_3$  and  $k_4$  determined by SECM.

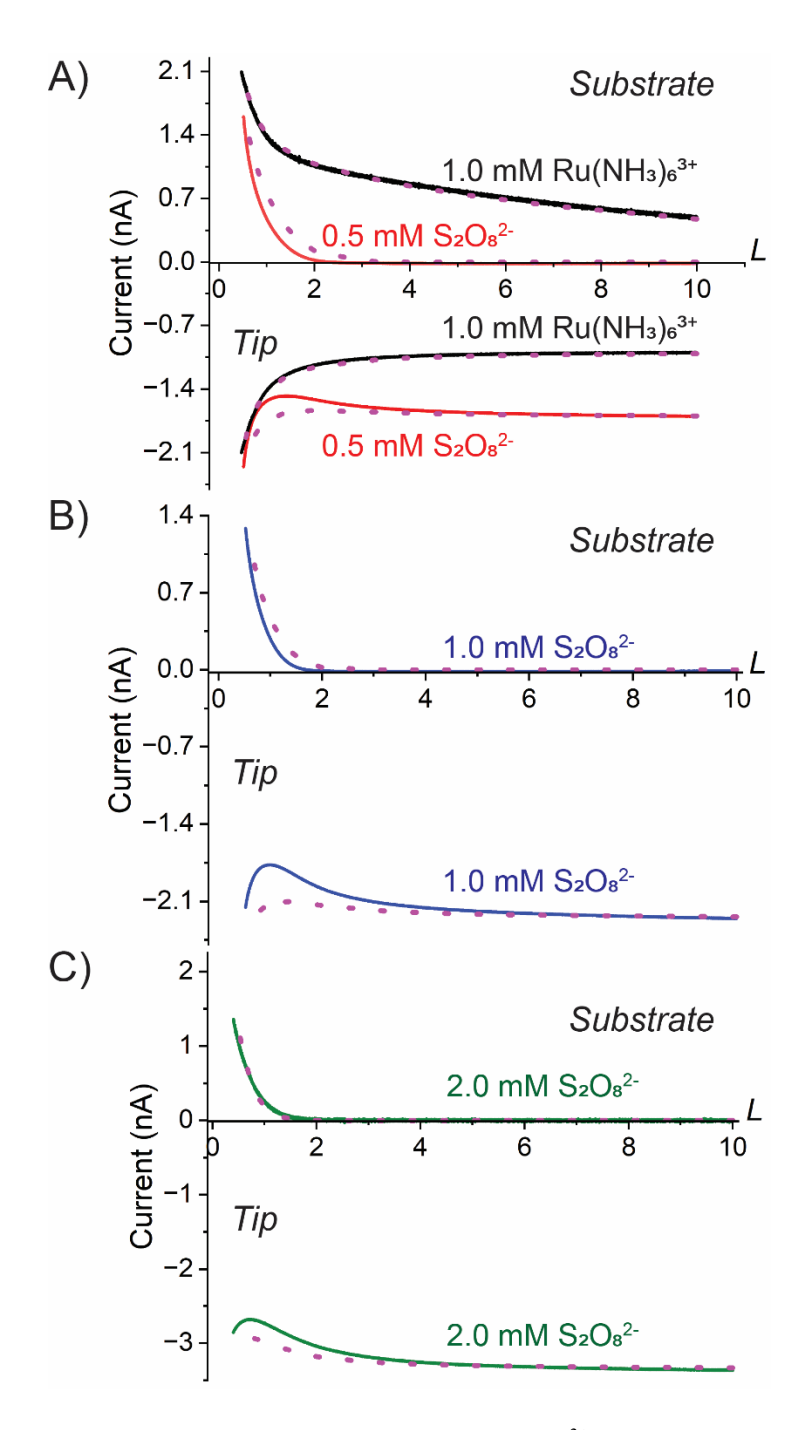


**Figure 7**. Experimental approach curves for A) 1.0 mM Ru(NH<sub>3</sub>) $_6^{3+}$  (black) and 1.0 mM Ru(NH<sub>3</sub>) $_6^{3+}$  with 0.50 mM S<sub>2</sub>O<sub>8</sub><sup>2-</sup> (red), B) 1.0 mM Ru(NH<sub>3</sub>) $_6^{3+}$  with 1.0 mM S<sub>2</sub>O<sub>8</sub><sup>2-</sup> (blue), and C) 1.0 mM Ru(NH<sub>3</sub>) $_6^{3+}$  with 2.0 mM S<sub>2</sub>O<sub>8</sub><sup>2-</sup> (green). Dotted magenta lines represent FEM simulation with  $k_3 = 1.0 \times 10^6$  s<sup>-1</sup>, and  $k_4 = 1.0 \times 10^9$  M<sup>-1</sup>s<sup>-1</sup>.  $k_2$  values of 5 × 10<sup>5</sup> M<sup>-1</sup>s<sup>-1</sup>, 6 × 10<sup>5</sup> M<sup>-1</sup>s<sup>-1</sup>, and 1 × 10<sup>6</sup> M<sup>-1</sup>s<sup>-1</sup> were employed for simulating approach curves at 0.50 mM, 1.0 mM, and 2.0 mM S<sub>2</sub>O<sub>8</sub><sup>2-</sup>, respectively. Approach curves were recorded using a 3.5-μm radius C-UME tip electrode (RG ~ 5) and a 25-μm radius (RG = 20) Pt-UME substrate electrode in an O<sub>2</sub>-free aqueous solution containing 0.1 M KCl (pH = 6.50).

# **Conclusion**

In the present work, we used SECM to investigate the kinetics of the elementary steps involved in the homogeneous reduction of  $S_2O_8^{2-}$ . The electrocatalytic reduction of  $S_2O_8^{2-}$  via  $Ru(NH_3)_6^{3+}$  includes five elementary steps in an aqueous solution. The average rate constant for the homogeneous reduction of  $S_2O_8^{2-}$  via electrogenerated  $Ru(NH_3)_6^{2+}$  was measured to be  $\sim 5 \times 10^5$  M<sup>-1</sup>s<sup>-1</sup> from SSV and  $\sim 7 \times 10^5$  M<sup>-1</sup>s<sup>-1</sup> from SECM measurements. Both values are slightly higher than previous findings based on CV ( $2 \times 10^5$  M<sup>-1</sup>s<sup>-1</sup>). Our SECM analysis is insensitive to values greater than  $1 \times 10^6$  s<sup>-1</sup> for the rate of  $S_2O_8^{3-}$  decomposition (i.e., eq. 3), which is also consistent with previous findings. Finally, a lower limit for the rate constant of the reaction between  $SO_4^{-}$  and  $Ru(NH_3)_6^{2+}$  was determined as  $\sim 1 \times 10^9$  M<sup>-1</sup>s<sup>-1</sup> using SECM measurements. This value is two orders of magnitude larger than previously reported and is consistent with values suggested by computations methods. Our investigate the kinetics of the elementary steps in the electrocatalytic reduction of  $S_2O_8^{2-}$  via electrogenerated  $S_2O_8^{2-}$  was measurements.

# **Associated Content**

Supporting Information is available free of charge at:

Details of steady-state voltammetry studies and parameters used for digital simulation of SSV, details of parameters used for simulation of SECM approach curves, and details of COMSOL model employed for simulation of steady-state voltammograms and approach curves.

# **Author Information**

Corresponding Authors

**Henry S. White** – Department of Chemistry, University of Utah, Salt Lake City, Utah, 84112, United States; orcid.org/0000-0002-5053-0996;

Email: white@chem.utah.edu; orcid.org/0000-0002-5053-0996

Authors

**Seyyedamirhossein Hosseini** — Department of Chemistry, University of Utah, Salt Lake City, Utah, 84112, United States; orcid.org/0000-0002-3617-2547

**Gergely T. Solymosi** – Department of Inorganic and Analytical Chemistry, Faculty of Chemical Technology and Biotechnology, Budapest University of Technology and Economics, Műegyetem rkp. 3, H-1111 Budapest, Hungary; orcid.org/0000-0003-4006-0326.

# **Notes**

The authors declare no competing financial interest.

# Acknowledgment

This work was supported by the National Science Foundation Center for Synthetic Organic Electrochemistry (CHE-2002158). GTS acknowledges a Fulbright Fellowship (AY2020-2021) for financial support of the visit to HSW's laboratory at the University of Utah.

# References

- 1. Zhou, M.; Li, C.; Luo, H.; Wang, J.; Sun, X. Electrooxidation of Sulfate aired to Electroreduction of Copper for Regeneration of Persulfate/Sulfuric Acid tching Solution. *Green Chem.* **2018**, *20*, 4710-4718.
- 2. Lee, J.;von Gunten, U.; Kim, J.-H. Persulfate-Based Advanced Oxidation: Critical Assessment of Opportunities and Roadblocks. *Envrion. Sci. Technol.* **2020**, *54*, 3064-3081.
- 3. Wang, B.; Wang, Y. A Comprehensive Review on Persulfate Activation Treatment of Wastewater. *Sci. Total Environ.* **2022,** *831*, 154906.

- 4. He, S.; Chen, Y.; Li, X.; Zeng, L.; Zhu, M. Heterogeneous Photocatalytic Activation of Persulfate for the Removal of Organic Contaminants in Water: A Critical Review. *ACS ES&T Engg.* **2022**, *2*, 527-546.
- 5. Armstrong, D. A.; Huie, R. E.; Koppenol, W. H.; Lymar, S. V.; Merényi, G.; Neta, P.; Ruscic, B.; Stanbury, D. M.; Steenken, S.; Wardman, P. Standard Electrode Potentials Involving Radicals in Aqueous Solution: Inorganic Radicals (IUPAC Technical Report). *Pure Appl. Chem.* **2015**, *87*, 1139-1150.
- 6. Chen, W.; Zheng, H.; Pan, X.; Xie, Z.; Zan, X.; Sun, B.; Liu, L.; Lou, H. A Metal-Free Cross-Dehydrogenative Coupling of N-Carbamoyl Tetrahydroisoquinoline by Sodium Persulfate. *Tetrahedron Lett.* **2014**, *55*, 2879-2882.
- 7. Karthikeyan, J.; Cheng, C.-H. Synthesis of Phenanthridinones from N-Methoxybenzamides and Arenes by Multiple Palladium-Catalyzed C-H Activation Steps at Room Temperature. *Angew. Chem., Int. Ed.* **2011,** *50*, 9880-9883.
- 8. Lee, M.; Sanford, M. S. Remote C(sp³)–H Oxygenation of Protonated Aliphatic Amines with Potassium Persulfate. *Org. Lett.* **2017**, *19*, 572-575.
- 9. Jin, J.; MacMillan, D. W. C. Direct α-Arylation of Ethers through the Combination of Photoredox-Mediated C-H Functionalization and the Minisci Reaction. *Angew. Chem., Int. Ed.* **2015**, *54*, 1565-1569.
- 10. Hosseini, S.; Janusz, J. N.; Tanwar, M.; Pendergast, A. D.; Neurock, M.; White, H. S. Oxidation by Reduction: Efficient and Selective Oxidation of Alcohols by the Electrocatalytic Reduction of Peroxydisulfate. *J. Am. Chem. Soc.* **2022**, *144*, 21103-21115.
- 11. Volpe, A.; Tubaro, C.; Natali, M.; Sartorel, A.; Brudvig, G. W.; Bonchio, M. Light-Driven Water Oxidation with the Ir-Blue Catalyst and the Ru(bpy)<sub>3</sub><sup>2+</sup>/S<sub>2</sub>O<sub>8</sub><sup>2-</sup> Cycle: Photogeneration of

- Active Dimers, Electron-Transfer Kinetics, and Light Synchronization for Oxygen Evolution with High Quantum Efficiency. *Inorg. Chem.* **2019**, *58*, 16537-16545.
- 12. Yu, X.-Y.; Bao, Z.-C.; Barker, J. R. Free Radical Reactions Involving Cl\*, Cl<sub>2</sub>-\*, and SO<sub>4</sub>-\* in the 248 nm Photolysis of Aqueous Solutions Containing S<sub>2</sub>O<sub>8</sub><sup>2</sup>- and Cl. *J. Phys. Chem. A.* **2004**, *108*, 295-308.
- 13. Wipf, D. O.; Kristensen, E. W.; Deakin, M. R.; Wightman, R. M. Fast-Scan Cyclic Voltammetry as a Method to Measure Rapid Heterogeneous Electron-Transfer Kinetics. *Anal. Chem.* **1988**, *60*, 306-310.
- 14. Polcari, D.; Dauphin-Ducharme, P.; Mauzeroll, J. Scanning Electrochemical Microscopy: A Comprehensive Review of Experimental Parameters from 1989 to 2015. *Chem. Rev.* **2016**, *116*, 13234-13278.
- 15. Cao, F.; Kim, J.; Bard, A. J. Detection of the Short-Lived Cation Radical Intermediate in the Electrochemical Oxidation of N, N-Dimethylaniline by Scanning Electrochemical Microscopy. *J. Am. Chem. Soc.* **2014**, *136*, 18163-18169.
- 16. Li, H.; Du, M.; Mleczko, M. J.; Koh, A. L.; Nishi, Y.; Pop, E.; Bard, A. J.; Zheng, X. Kinetic Study of Hydrogen Evolution Reaction Over Strained MoS<sub>2</sub> with Sulfur Vacancies Using Scanning Electrochemical Microscopy. *J. Am. Chem. Soc.* **2016**, *138*, 5123-5129.
- 17. Zhou, F.; Unwin, P. R.; Bard, A. J., Scanning Electrochemical Microscopy. 16. Study of Second-Order Homogeneous Chemical Reactions via the Feedback and Generation/Collection Modes. *J. Phys. Chem.* **1992**, *96*, 4917-4924.
- 18. Kai, T.; Zhou, M.; Duan, Z.; Henkelman, G. A.; Bard, A. J. Detection of CO<sub>2</sub> in the Electrochemical Reduction of Carbon Dioxide in N,N-Dimethylformamide by Scanning Electrochemical Microscopy. *J. Am. Chem. Soc.* **2017**, *139*, 18552-18557.

- 19. Kai, T.; Zhou, M.; Johnson, S.; Ahn, H. S.; Bard, A. J. Direct Observation of C<sub>2</sub>O<sub>4</sub><sup>-</sup> and CO<sub>2</sub><sup>-</sup> by Oxidation of Oxalate within Nanogap of Scanning Electrochemical Microscope. *J. Am. Chem. Soc.* **2018**, *140*, 16178-16183.
- 20. Rodríguez-López, J.; Shen, M.; Nepomnyashchii, A. B.; Bard, A. J. Scanning Electrochemical Microscopy Study of Ion AnnihilationElectrogenerated Chemiluminescence of Rubrene and [Ru(bpy)<sub>3</sub>]<sup>2+</sup>. *J. Am. Chem. Soc.* **2012**, *134*, 9240–9250
- 21. Bard, A. J.; Mirkin, M. V. *Scanning lectrochemical Microscopy*, 3<sup>rd</sup> Ed.; CRC Press: Boca Raton, 2022.
- 22. Najarian, M. A.; Chen, R.; Balla, R. J.; Amemiya, S.; McCreery, R. L. Ultraflat, Pristine, and Robust Carbon Electrode for Fast Electron-Transfer Kinetics. *Anal. Chem.* **2017**, *89*, 13532-13540.
- 23. Bhat, M. A.; Nioradze, N.; Kim, J.; Amemiya, S.; Bard, A. J. In Situ Detection of the Adsorbed Fe(II) Intermediate and the Mechanism of Magnetite Electrodeposition by Scanning Electrochemical Microscopy. *J. Am. Chem. Soc.* **2017**, *139*, 15891-15899.
- 24. Martin, R. D.; Unwin, P. R. Scanning Electrochemical Microscopy Kinetics of Chemical Reactions Following lectron-tranTsfer Measured with the Substrate-Generation–Tip-ollection Mode. *J. Chem. Soc., Faraday Trans.* **1998**, *94*, 753-759.
- 25. Mirkin, M. V.; Yang, H.; Bard, A. J. Borohydride Oxidation at a Gold Electrode. *J. Electrochem. Soc.* **1992**, *139*, 2212.
- 26. Danis, L.; Polcari, D.; Kwan, A.; Gateman, S. M.; Mauzeroll, J. Fabrication of Carbon, Gold, Platinum, Silver, and Mercury Ultramicroelectrodes with Controlled Geometry. *Anal. Chem.* **2015**, *87*, 2565-2569.

- 27. Gao, R.; Edwards, M. A.; Qiu, Y.; Barman, K.; White, H. S. Visualization of Hydrogen Evolution at Individual Platinum Nanoparticles at a Buried Interface. *J. Am. Chem. Soc.* **2020**, *142*, 8890-8896.
- 28. https://warwick.ac.uk/fac/sci/chemistry/research/electrochemistry/home/
- 29. Wang, Y.; Limon-Peterson, J. G.; Compton, R. C. Measurement of the Diffusion Coefficients of [Ru(NH<sub>3</sub>)<sub>6</sub>]<sup>3+</sup> and [Ru(NH<sub>3</sub>)<sub>6</sub>]<sup>2+</sup> in Aqueous Solution Using Microelectrode Double Potential Step Chronoamperometry. *J. Electroanal. Chem.* **2011**, *652*, 13-17.
- 30. White, H. S.; Becker, W. G.; Bard, A. J. Photochemistry of the Tris(2,2'-Bipyridine)Ruthenium(II)-Peroxydisulfate System in Aqueous and Mixed Acetonitrile-Water Solutions. Evidence for a Long-Lived Photoexcited Ion Pair. *J. Phys. Chem.* **1984**, *88*,1840-1846.

# For Table of Contents Only

